# Single-Site Vanadyl Activation, Functionalization, and Reoxidation Reaction Mechanism for Propane Oxidative Dehydrogenation on the Cubic $V_4O_{10}$ Cluster

**Mu-Jeng Cheng, Kimberly Chenoweth, Jonas Oxgaard, Adri van Duin, and William A. Goddard, III***

*Materials and Process Simulation Center (139-74), California Institute of Technology, Pasadena, California 91125*

*Received: September 28, 2006; In Final Form: January 10, 2007*

Vanadyl oxide (V═O) sites are thought to play a role in a number of industrially important catalysts for activating saturated alkanes, but in no system is the mechanism for the activation, product formation, and reoxidation steps established. In this paper, we use quantum mechanical methods (B3LYP flavor of density functional theory) to examine the detailed mechanism for propane reacting with a $V_4O_{10}$ cluster to model the catalytic oxidative dehydrogenation (ODH) of propane on the $V_2O_5$(001) surface. We here report the mechanism of the complete catalytic cycle, including the regeneration of the reduced catalyst using gaseous $O_2$. The rate-determining step is hydrogen abstraction by the vanadyl (V═O) group (in agreement with experiment) to form an iso-propyl radical that binds to an adjacent V−O−V site. Subsequently, this bound iso-propyl forms propene product by $\beta$-hydride elimination to form bound $H_2O$. We find that this $H_2O$ (bound to a $V^{III}$ site) is too stable to desorb unimolecularly. Instead, the desorption is induced by binding of gaseous $O_2$ to the $V^{III}$ site, which dramatically decreases the coordination energy of $H_2O$ from 37.8 to 12.9 kcal/mol. Further rearrangement of the $O_2$ molecule leads to formation of a cyclic $VO_2$ peroxide, which activates the C−H bond of a second propane to form a second propene (with a lower reaction barrier). Desorption of this propene regenerates the original $V_4O_{10}$ cluster. We find that all reactions involve the single vanadyl oxygen (V═O), with the bridging oxygens (V−O−V) serving to stabilize the iso-propyl radical intermediate. We refer to this mechanism as the single-site vanadyl activation, functionalization, and reoxidation mechanism (SS-VAFR). This SS-VAFR mechanism should be applicable to propane ODH on the supported vanadium oxide catalysts where only monovanadate ($VO_4$) species are present.

## 1. Introduction

Selective oxidation of saturated hydrocarbons (ethane, propane, butane) to feedstocks for polymers and chemicals is increasingly important for both economic and environmental reasons. However, activation and selective production of products has been much more of a challenge for these saturated hydrocarbons than for unsaturated systems (ethene, propene, butene). Even so, industrially successful heterogeneous catalysts have been developed, including vanadyl pyrophosphate (VPO) for conversion of butane to maleic anhydride, and mixed metal oxide (MMO) catalysts for selective oxidation and ammoxidation of propene to acrolein and acrylonitrile. In all of these systems, there is considerable uncertainty about the detailed chemical mechanism involved, which has made improvements and optimization difficult. Characteristic of the catalysts listed above is the use of vanadyl oxide to activate the very strong bond of the saturated alkanes. As a starting point for determining the mechanism, we chose to start with $V_2O_5$ and the oxidative dehydrogenation of propane to propene.

Dehydrogenation of alkanes to give the corresponding alkenes and $H_2$ is strongly endothermic and can be carried out only at temperatures above 900 K.[1−3] In addition to being uneconomical, these high reaction temperatures cause unwanted side reactions, leading to coke formation. In contrast, the oxidative dehydrogenation (ODH) reaction

$$CH_3{-}CH_2{-}CH_3 + {}^1/_2O_2 \rightarrow CH_3{-}CH{=}CH_2 + H_2O$$

is an attractive alternative to simple dehydrogenation, because it is exothermic due to the formation of water.[1] However, a selective catalyst is required to avoid complete oxidation to $CO_2$ and CO. Currently, the best alkane ODH catalysts contain either dispersed vanadia or particles of $V_2O_5$ that have a variety of vanadium coordination geometries and oxidation states, ranging from $2^+$ to $5^+$ (currently no supported $V_2O_5$ catalysts are in commercial use).[3]

Figure 1 shows the structure of the $V_2O_5$ (001) surface, the most stable surface of the bulk $V_2O_5$. This surface includes three types of oxygen atoms: (1) O(1) is bonded to one V, forming a double bond, with a bond distance of V═O(1) = 1.58 Å. (2) O(2) is bonded to two V, forming two single bonds: V−O(2)−V with bond lengths of V−O(2) = 1.78 Å. (3) O(3) is coordinated to three V but with two bond V−O(3) distances of 1.88 Å, somewhat longer than a single bond (1.78 Å) and one much longer distance (V−O(3) = 2.02 Å), which we consider as a donor−acceptor or coordination bond.

Experimental studies have provided some insight into the mechanism of alkane ODH.[1−16] Most studies have focused on the alkane ODH on supported vanadium oxides rather than bulk $V_2O_5$, because highly dispersed vanadium oxides on supports display higher selectivity (29−90%) than the bulk $V_2O_5$ (18−31%).[2,3,11,17] Went et al.[4] used laser Raman spectroscopy to investigate supported vanadium oxide catalysts ($V_2O_5/SiO_2$,

* Corresponding author. E-mail: wag@wag.caltech.edu.

10.1021/jp0663917 CCC: $37.00 
Published on Web 03/14/2007

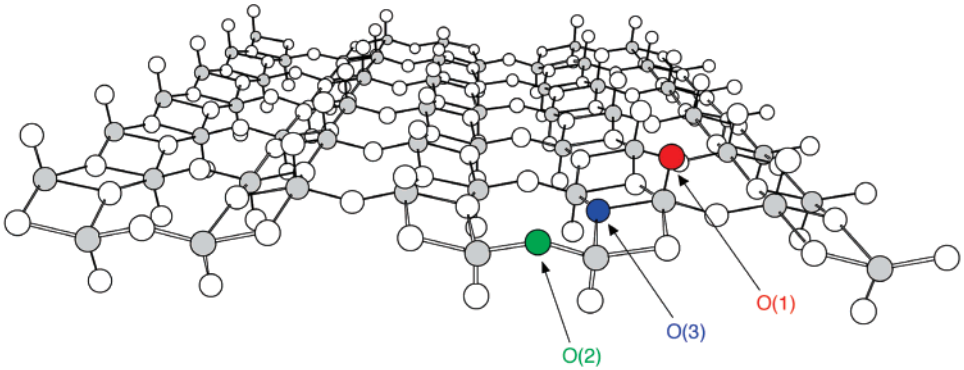


**Figure 1.** The three types of oxygen atoms on the $V_2O_5(001)$ surface where the vanadium atoms are shown in gray and oxygen atoms are represented as white circles. The bonding types V═O(1), V−O(2)−V are in the $V_4O_{10}$ cluster, but not the O(3).

$V_2O_5/TiO_2$, and $V_2O_5/Al_2O_3$) and found that three vanadia species, monovanadate, one- and two-dimensional vanadate chains (polyvanadate), and crystallites of $V_2O_5$ were present on the supports depending on the $V_2O_5$ loading, which has been confirmed in more recent experimental results.[11] On the basis of the relationship between the ethylene turnover rate and vanadium oxide concentration on an $SiO_2$ support, Oyama[7] concluded that only a single vanadium center is necessary for ethane ODH. These conclusions are consistent with the results obtained by Busca et al.[10] and Kung.[9] Recently, Pieck et al.[16] studied propane ODH on $V_2O_5/ZrO_2$ catalysts and showed that monovanadates have both higher activity and better selectivity to propene than bulk $V_2O_5$ and polyvanadates. In contrast, Khodakov et al.[11] found that the polyvanadate structures are significantly more active than monovanadate structure. It is not clear whether the ODH reaction occurs on mono- or polyvanadate sites, but it appears likely that these sites are more important than crystalline $V_2O_5$.

Several studies give hints about the individual steps. Le Bars et al.[8] carried out a calorimetric experiment of ethane ODH on unsupported $V_2O_5$ to show that $O_2$ is important in regenerating the vanadia surface and maintaining a high olefin yield, most likely by keeping vanadium in its highest oxidation state. Chen et al.[12,13] used deuterium and $^{13}C$ isotopes to study the reaction pathways of propane ODH on $V_2O_5/ZrO_2$ catalysts. They determined that the C−H bond activation step is irreversible and that the methylene C−H bond of propane is activated in the rate-determining step.[12,13] Argyle et al.[14,15] measured the activation barrier for both propane and ethane ODH on alumina-supported vanadia and found both to be 27 kcal/mol. It has generally been assumed that the oxygen reacting with the alkane comes from the lattice and the reduced catalyst is reoxidized by gaseous $O_2$, which is referred to as a Mars−van Krevelen model.[12,13,18,19] Computational studies on related systems reported by Gilardoni et al.,[20] Redfern et al.,[21] and Fu et al.[22] are described in the discussion section.

Because of the considerable uncertainties in the details of the reaction mechanism for these systems, we determined the propane ODH mechanisms on the cubic $V_4O_{10}$ cluster (Figure 2). We examined both the mechanism for activating the C−H bond of propane with subsequent formation of propene and the mechanism for reoxidation of the reduced vanadium oxide catalyst.

Although we believe that most of the chemistry of the $V_2O_5$-(001) surface is captured by the $V_4O_{10}$ model, it is not a perfect model of this surface because it contains only O(1) and O(2) like oxygens. However, we believe that the results from the $V_4O_{10}$ model are directly applicable to mechanisms for supported vanadia catalysts, where the relevant chemistry must happen at a single site.

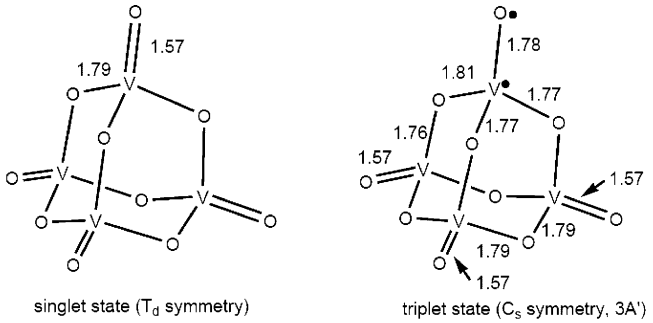


**Figure 2.** Structural parameters for the singlet state and triplet state of $V_4O_{10}$ cluster. The singlet state has $T_d$ symmetry; the triplet state has $C_s$ symmetry ($^3A'$).

In particular, this paper aims to answer the following questions: (1) How do the structural parameters, vibrational spectra, and electronic states of the $V_4O_{10}$ cluster compare to the $V_2O_5$ (001) surface? (2) What is the mechanism for C−H activation of alkanes? (3) What are the subsequent steps for formation of propene and $H_2O$ products? (4) By what mechanism is the surface reoxidized? (5) Can we find a coherent mechanistic cycle from theory that is consistent with available experimental results on the $V_2O_5$ crystal?

## 2. Computational Details

Our DFT calculations used the B3LYP functional,[23] which combines exact HF exchange with the Becke generalized gradient exchange functional of Becke[24] (B) and the Lee, Yang, and Parr[25] (LYP) correlation functional. This functional is known to provide a good description of the potential energy surface (PES) of transition metal-containing compounds.[26−36] The metals were described using the Wadt and Hay[37] core-valence (relativistic) effective core potential (treating the 13 3s, 3p, 3d, 4s, 4p electrons of V explicitly) with the valence double-ζ contraction of the basis functions (denoted as LACVP** in Jaguar). All electrons were included on the H, C, and O atoms using a modified variant of the Pople[38,39] 6-31G** basis set.

The analytic Hessian was calculated for each local minimum and each transition state and used to calculate the vibrational frequencies. We ensured that each local minimum had zero imaginary frequencies, while each transition state structure had one imaginary frequency. These vibrational frequencies were used to calculate the zero-point energy (ZPE) to obtain enthalpies at 0 K for each structure and to calculate the enthalpy and

entropy corrections to obtain the Gibbs free energy at 298.15 K. All calculations were performed using the Jaguar 6.5 program package.[40]

The units used here for bond lengths, bond angles, and energetic parameters are Å, degree, and kcal/mol, respectively. The Cartesian coordinates as well as the total energies for the structures in the paper have been provided in the Supporting Information.

## 3. Results

**3.1. $V_4O_{10}$ Cluster Model.** The $V_4O_{10}$ (**1**) cluster in Figure 2 can be considered as a topological equivalent of the top surface layer of the $V_2O_5$ (001) surface mapped onto a sphere. This cluster contains the vanadyl V═O(1) site and the V−O(2)−V site, but does not contain the 3-fold coordinated oxygen O(3) site. However, the crystal structure[41] shows that this site has two short V−O(3) bonds of 1.88 Å, similar to the V−O(2) bonds (1.78 Å), which we consider as partially ionic−covalent bonds, while the third V−O(3) bond length is 2.02 Å, which we consider as a donor−acceptor bond. This means that O(3) is connected with two covalent bonds instead of three. Therefore, we consider the $V_2O_5$ (001) surface to have one V═O(1) bond and three V−O(2) bonds, making it structurally similar to our $V_4O_{10}$ cluster model. All vanadium atoms in $V_4O_{10}$ have a formal oxidation state of $5^+$, with each vanadium atom connected through an O(2) to three $V^V$. Thus, we consider the $V_4O_{10}$ cluster suitable for modeling the chemistry of the $V_2O_5$-(001) surface.

Figure 2 shows the structural parameters of the singlet of $V_4O_{10}$ (**1**). The bond distances are V═O(1) = 1.57 Å and V−O(2) = 1.79 Å, in good agreement with the experimental values of V═O = 1.58 Å and V−O = 1.78 Å obtained for the bulk $V_2O_5$.[41] Periodic DFT calculations on the $V_2O_5$(001) surface also lead to V═O = 1.59 Å and V−O = 1.80 Å.[42]

We consider that the V═O(1) bond involves 6 electrons: 2 from the V [say in the $(d_{xz})(d_{yz})$ configuration] and 4 from the O [say in the $(p_z)^2(p_x)(p_y)$ configuration], leading to a bond that can be considered as a double bond plus a donor acceptor bond. Thus, the ground state is $(\sigma)^2(\pi_x)^2(\pi_y)^2$, where $\sigma$ has $a_1$ symmetry and $(\pi_x,\pi_y)$ belongs to the e irreducible representation, in the $C_{3v}$ point group. Thus, we will write this configuration as $(\sigma)^2$-$(\pi)$.[4] We then consider that each V makes three somewhat polar covalent bonds to the three O(2) neighbors.

The Mulliken populations of $V_4O_{10}$ are $Q_V = 1.41$, $Q_{O(1)} = -0.31$, and $Q_{O(2)} = -0.73$ electrons. This is in good agreement with the values of $Q_V = 1.46$, $Q_{O(1)} = -0.39$, and $Q_{O(2)} = -0.71$ electrons derived from analyzing the electrostatic fields. Thus, each V−O(2) bond can be considered to have a charge transfer of 0.37 $e^-$ from V to O, while the net transfer in the V═O(1) bond is only 0.31 $e^-$ despite two partially polar covalent bonds. This is because of back transfer in the donor−acceptor bond. We should point out that the small charge transfer from V to O is due to the high oxidation state. For the V═O diatomic, we would expect more charge transfer. We calculate four vibrational frequencies in the range of 1126−1149 $cm^{-1}$ for the V═O(1) bond stretch, consistent with experimental values of 1040 $cm^{-1}$ for bulk $V_2O_5$,[43] 1010 $cm^{-1}$ for $V_2O_5/ZrO_2$,[16] and 1042 $cm^{-1}$ for $V_2O_5/SiO_2$.[44]

We also calculated the triplet state of $V_4O_{10}$. Here, we expect a $\pi \rightarrow \pi^*$ transition (that is, e → e*) in one of the V═O(1) bonds, leading to a $(\sigma)^2(\pi)^3(\pi^*)^1$ configuration. For the $C_{\infty v}$ point group, this would lead to four states: $^3\Sigma^+$, $^3\Delta$, and $^3\Sigma^-$ (in increasing energy), which become $^3A_1$, $^3E$, and $^3A_2$ in $C_{3v}$. Thus, the lowest triplet state would lead to a distortion from the $T_d$ symmetry of the ground state to $C_{3v}$. However, to obtain these correct symmetries requires two configuration wave functions (e.g., $[\pi_x^2\pi_y\pi_y^* + \pi_x\pi_x^*\pi_y^2]$). Our QM calculations use a single configuration and hence would mix the $^3\Sigma^+$ and $^3\Delta^+$ states, which should lower the symmetry to $C_s$, with degenerate states of the A′ and A″ irreducible representation.

The triplet state has both unpaired electrons localized on one V═O(1) group, as expected, with 0.75 unpaired spin on the V atom and 0.94 unpaired spin on the O(1) atom, consistent with slight polarity in the bond. This V═O(1) bond elongates from 1.57 to 1.78 Å, as expected because the total bond order is 1 rather than 2. [The other V═O(1) bond lengths do not change from the value in the singlet state.] In addition, the distance of one of the three V−O(2) bonded to the excited V═O increases to 1.81 Å, while the other two decrease to 1.77 Å (Figure 2).

The singlet−triplet gap is $\Delta E_{S-T} = E_{triplet} - E_{singlet} = 47.2$ kcal/mol, which is 12% lower than the experimental band gap for $V_2O_5$ crystal of 53.0−54.4 kcal/mol.[45,46] This may be because the $V_4O_{10}$ cluster permits the triplet state to relax more completely than in the bulk crystal. Indeed, using the ground-state geometry, vertical triplet excitation energy is 61.6 kcal/mol, suggesting that the relaxation is responsible for this discrepancy. On the basis of the structural and energetic similarities of the $V_4O_{10}$ cluster to $V_2O_5$ (001), we conclude that the $V_4O_{10}$ cluster is a plausible model both for studying the initial C−H activation of alkane ODH reaction on $V_2O_5$ (001) surface and for gaining insight into the whole mechanism.

**3.2. C−H Bond Activation.** To reduce computational expense, the initial investigations on C−H activation were performed with the smaller $CH_4$ system. Four possible mechanisms of C−H bond activation were studied, including two types of addition reactions, which involve heterolytic C−H bond cleavage, and two types of hydrogen abstraction reactions, which involve homolytic C−H bond cleavage. The optimized geometries and the calculated energies of the four pathways are summarized in Figure 3.

Path A involves an addition reaction utilizing the V═O(1) group, where the methyl group binds to O(1) and the hydrogen atom binds to the V atom. In the transition state structure (TsA), the V═O(1) bond elongates from 1.57 to 1.64 Å; the C−H bond distance of methane elongates from 1.11 to 1.82 Å. The $CH_3$−O(1) and H−V bond distances are 1.99 and 1.62 Å, respectively. Vanadium hydride and an adsorbed methoxy are formed in the product (ProA) with $CH_3$−O(1), H−V, and V−O(1) bond distances of 1.43, 1.58, and 1.71 Å, respectively. Two of the three V−O(2) bond distances increase to 1.89 and 1.85 Å, while the other decreases to 1.75 Å. The activation barrier for Path A is 85.3 kcal/mol, which is the highest among the four pathways discussed here.

Path B is also a V═O(1) addition reaction, but with the methyl group attaching to the vanadium atom and the hydrogen atom attaching to the O(1) atom. In the transition state (TsB), the V═O(1), C−H, H−O(1), and $CH_3$−V bond distances are 1.68, 1.56, 1.13, and 2.42 Å, respectively. Vanadium carbide and an adsorbed hydroxyl are formed in the product, ProB, with V═O(1), H−O(1), and $CH_3$−V bond distances of 1.75, 0.97, and 2.05 Å, respectively. A significant structural change was observed where one of the three V−O(2) bonds elongates to 1.98 Å, while the other two bond distances are 1.73 and 1.80 Å, similar to those of the $V_4O_{10}$ reactant. The barrier for Path B is still quite high (51.6 kcal/mol), but it has a much lower

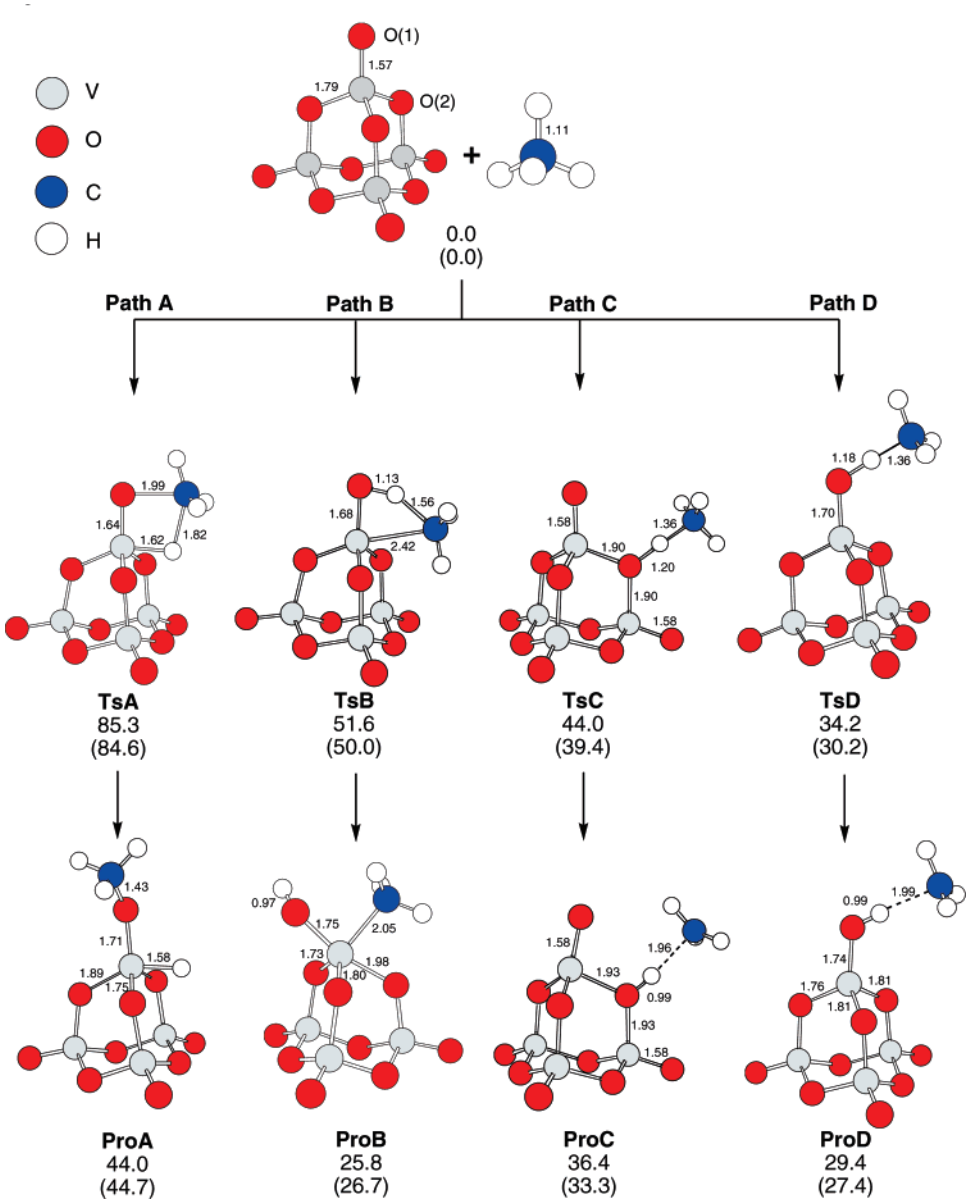


**Figure 3.** Reaction pathways and energies ($\Delta E$) for initial C−H bond activation of methane (the number in parentheses is $\Delta H_{0K} = \Delta E + \text{ZPE}$). The H abstraction by V═O(1), Path D, is clearly the most favorable process, although ProB is lower than ProD.

barrier than Path A due to better electrostatic interactions ($V^{\delta+}-C^{\delta-}$ and $O^{\delta-}-H^{\delta+}$). Nevertheless, we conclude that the V═O(1) addition reactions are sufficiently unfavorable energetically that they need not be considered for the alkane ODH reaction mechanism.

Paths C and D involve hydrogen abstraction reactions. Both reactions led to transition states and products having diradicaloid electronic structures, which we described as open-shell singlet states. In Path C, the bridging oxygen O(2) abstracts the hydrogen atom from methane. The O(2)−H and H−$CH_3$ bond distances in the transition state (TsC) are 1.20 and 1.36 Å, respectively. The bond distances between the O(2) and the two neighbor V atoms are both 1.90 Å, which are 0.11 Å longer than those in the $V_4O_{10}$ structure. There is no significant change in the four V═O(1) bond distances. The $\langle S^2 \rangle$ is equal to 0.83, indicating a slight correlation of the spins, but overall we consider this state as diradicaloid. The structure of the product (ProC) is very similar to that of TsC but with the O(2)−H bond decreased to 0.99 Å and the H−$CH_3$ distance increased to 1.96 Å. It can be described as a radical pair with very weak interactions between the two radical fragments, with $\langle S^2 \rangle = 1.05$. We also calculated the true triplet state of ProC and found that both the structure and the energy are almost identical to the singlet (RMSD of singlet/triplet bonds = 0.0002 Å, triplet energy is 0.02 kcal/mol lower than the singlet energy). The reaction barrier for Path C is 44.0 kcal/mol, which is 7.6 kcal/mol lower than Path B (and 41.3 kcal/mol lower than Path A).

Path D uses the terminal oxygen O(1) to abstract the hydrogen atom from methane, going through transition state structure TsD, where V−O(1) = 1.70, O(1)−H = 1.18, and H−$CH_3$ = 1.36 Å. The corresponding product (ProD) has bond distances of V═O(1) = 1.74, O(1)−H = 0.99, and H−$CH_3$ = 1.99 Å. Both TsD and ProD have a nonzero $\langle S^2 \rangle$ (0.82 for TsD and 1.01 for ProD), similar to the corresponding values in Path C. Thus, TsD is a diradicaloid structure, while ProD is a radical-paired molecule very similar to the corresponding triplet state (RMSD of singlet/triplet bond lengths = 0.002 Å; the triplet energy is 0.3 kcal/mol higher than the singlet energy). The activation barrier for this pathway is only 34.2 kcal/mol, which is the most energetically favorable pathway among the four reactions studied

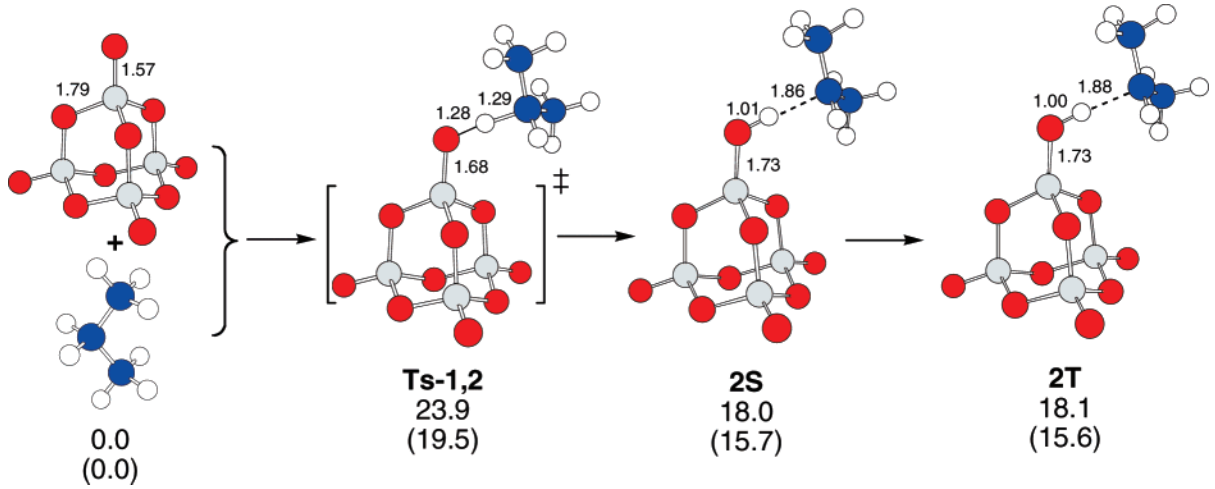


**Figure 4.** The first and second steps of propane ODH on $V_4O_{10}$ (the first row of the energetic parameters is $\Delta E$, while the second row is $\Delta H_{0K} = \Delta E + \text{ZPE}$). The near degeneracy of **2S** and **2T** demonstrates the diradical character of this state (one unpaired spin on the $\beta$ carbon and one on the V).

here. This should be contrasted with the reaction of methane with $V_4O_{10}^+$ investigated by Feyel et al.,[47] where there is no barrier for the hydrogen migration from methane to O(1). This indicates that the chemistry is very different between cationic and neutral $V_4O_{10}$.

Thus, we conclude that hydrogen abstraction pathways are much more favorable than the addition pathways. This is reasonable because the $\pi$ bond of V═O(1) has a singly occupied orbital available to bond to the H and pointing toward it, whereas for O(2) the orbital overlapping the H is a filled lone pair orbital. In addition, the hydrogen abstraction reactions have the $\sigma$-orbital of C−H bond aligned with the lone pair electrons orbital of O(1) or O(2), so that there is no orbital alteration during the reaction process. In contrast, the addition reaction requires the $\sigma$-orbital of C−H bond in methane to break almost completely before it can overlap with the filled lone pair orbital on oxygen and the empty d-orbital on vanadium, leading to a high barrier. On the basis of the C−H activation of methane on the $V_4O_{10}$ model, we conclude that hydrogen abstraction by O(1) is the most likely first step for alkane ODH reaction on the $V_2O_5$-(001) surface, and thus we consider it as the initial step for the propane ODH mechanism.

**3.3. Oxidative Dehydrogenation of Propane on $V_4O_{10}$.** Next, we consider the propane ODH reaction on $V_4O_{10}$ leading to propene and $V_4O_{10}H_2$. We consider four important steps for each possible reaction pathway. (1) Vanadyl-$H^{1st}$-abs: A hydrogen atom is abstracted from the methylene group in propane by V═O(1) to form a singlet radical-paired intermediate. (2) Spin conversion: The electronic state of the intermediate changes from the singlet to the energetically nearly degenerate triplet state ($\Delta E_{S-T} \approx 0.1$ kcal/mol). (3) Radical trapping: The iso-propyl radical bonds with one of the oxygens [O(1)H or O(2)] to form a triplet intermediate. (4) Propene formation: O(2), O(1)H, or O(1) is used to abstract the second hydrogen from a methyl group to form propene and $V_4O_{10}H_2$.

The energetics and structures for steps 1 and 2 are summarized in Figure 4, while the results for steps 3 and 4 are shown in Figure 5. Figure 6 shows the potential energy surfaces of the three possible reaction pathways.

On the basis of the barriers for C−H activation in methane, we expect the initial step in propane ODH to be hydrogen abstraction of the methylene hydrogen from propane by the V═O(1) site, producing an iso-propyl radical (vanadyl-$H^{1st}$-abs step). We calculate an activation energy for this reaction of 23.9 kcal/mol, which is in good agreement with the experimental barrier of propane ODH on supported vanadium oxides ($E_a$ = 27.0 kcal/mol).[14,15]

In Path 1 (Figure 5), the iso-propyl radical binds to the O(1)H group to form **3A**, which is 34.4 kcal/mol more stable than **2T**. **3A** is a triplet state lying 24.8 kcal/mol below the corresponding singlet state and can be considered a complex of iso-propanol and the triplet $V_4O_9$ cluster with two unpaired electrons located on the vanadium atom that bonds with iso-propanol. (The $V_4O_9$−iso-propanol bond distance is 2.01 Å.) In the final step in Path 1, O(2) abstracts the second hydrogen from the methyl group, leading to propene and **4A**, with an activation barrier of 31.2 kcal/mol.

Paths 2 and 3 start with the formation of the same intermediate (**3B**), through a bond formed between the iso-propyl radical and O(2). Similar to **3A**, **3B** is a triplet state lying 19.4 kcal/mol below the corresponding singlet state. Spin density analysis of **3B** shows that the two unpaired electrons are located on the same vanadium atom bonded to the hydroxyl group. In Path 2, O(1) abstracts an hydrogen from the methyl group with a 31.2 kcal/mol barrier (**Ts-3B,4B**) to form propene and **4B**.

Path 3 (hydroxyl-$H^{2nd}$-abs step), starting from the same intermediate, **3B**, uses the O(1)H group to abstract a hydrogen atom from the methyl group, leading to the formation of propene and **4C**, with a 30.8 kcal/mol barrier (**Ts-3B,4C**). We find that the spin distribution of **Ts-3B,4C** is the same as in **3B**. In the **Ts-3B,4C** structure, the bond distance of V−O(1)H increases from 1.79 Å in **3B** to 1.88 Å, while the V−O(2) bond distance decreases from 2.03 to 1.90 Å. For the product **4C**, spin density analysis shows that the two unpaired electrons are located on the same V atom bonded to the water fragment, which is similar to **3B** and **Ts-3B,4C**. Therefore, **4C** can be considered a complex of water and triplet $V_4O_9$, with a 2.05 Å bond distance between the two fragments.

Path 3 has the lowest reaction barrier among the three possible reaction pathways studied in this work, 30.8 kcal/mol. The similar activation energies of Path 2 and Path 3 imply that O(1) and O(1)H have very similar nucleophilic characteristics, which contradicts the prediction by Chen[9,10] that a new O(1) is needed to abstract the second hydrogen atom. We will use this lowest energy pathway, Path 3, in the next section to study the catalytic cycle for propane ODH.

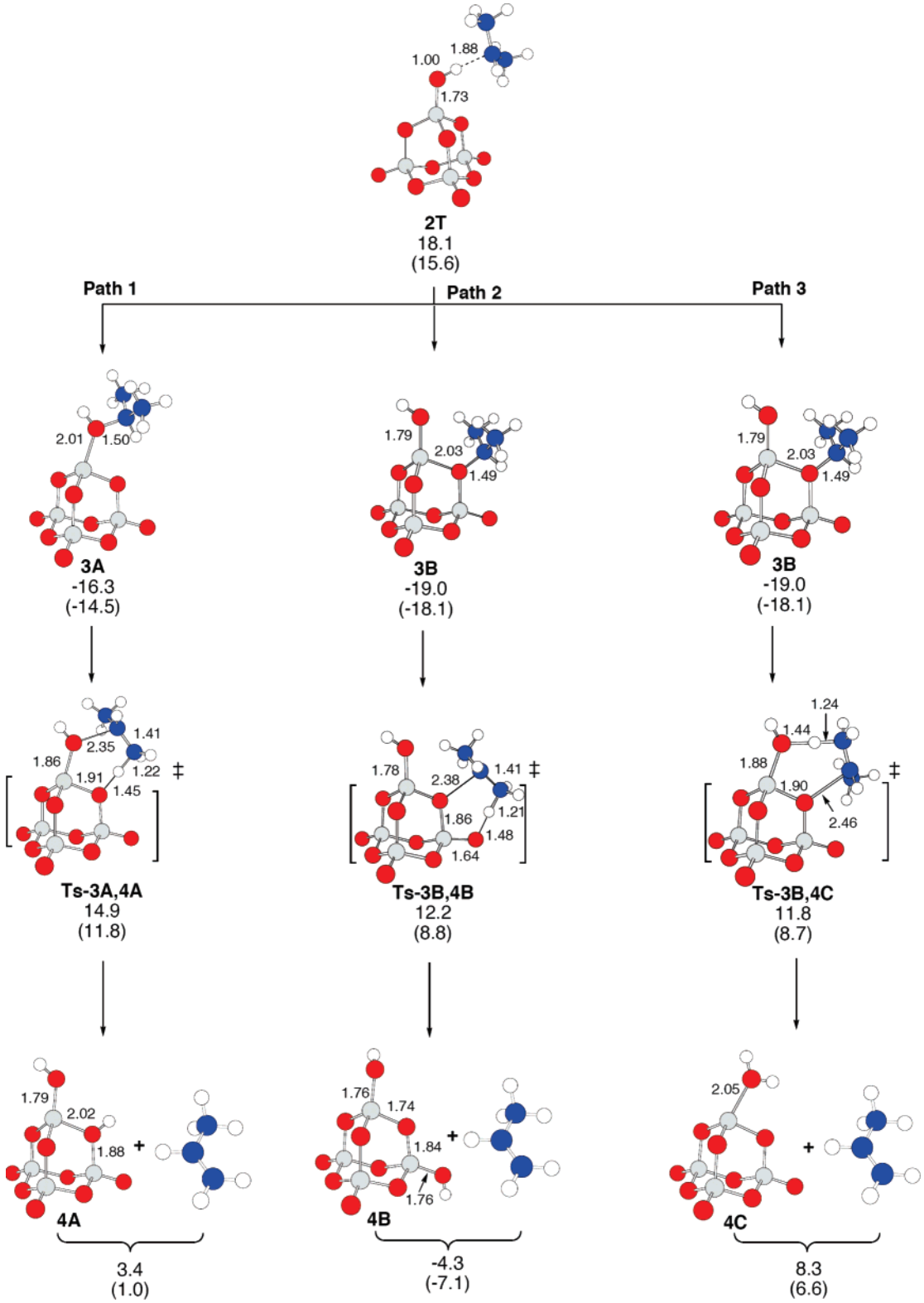


**Figure 5.** The three pathways for binding of iso-propyl radical (iPr) to the $V_4O_{10}$ followed by the second hydrogen abstraction to release the propene product (the first row of the energetic parameters is $\Delta E$, while the second row is $\Delta H_{0K} = \Delta E + \text{ZPE}$). The first step is favorable for all cases, but the barrier from this step to the next one ($\Delta H_{0K} = 26.3$, 26.9, and 26.8, respectively) argues against Path2. We favor Path3 because it leads to a bound $H_2O$ product (rather than two isolated OH groups), which might more easily be removed to recycle the catalyst. Also, Path3 can occur at isolated sites.

**3.4. Vanadium Reoxidation.** The optimized structures of the intermediates and products on the reaction pathways discussed below are summarized in Figure 7. The most favorable steps lead to **4C**, which we now consider as the starting point for the final part of the mechanism, dissociation of product and catalyst reoxidation. Recall that **4C** is a triplet state with the $H_2O$ bound through the lone pair of O. Considering the $VOH_2$ plane as *yz* with the *z*-axis pointing along the axis of the $V_4O_9$ cluster, the $V-OH_2$ bond distance is 2.05 Å (a donor−acceptor bond), with an angle of 30.1° from the *z*-axis. Thus, the O lone pair is

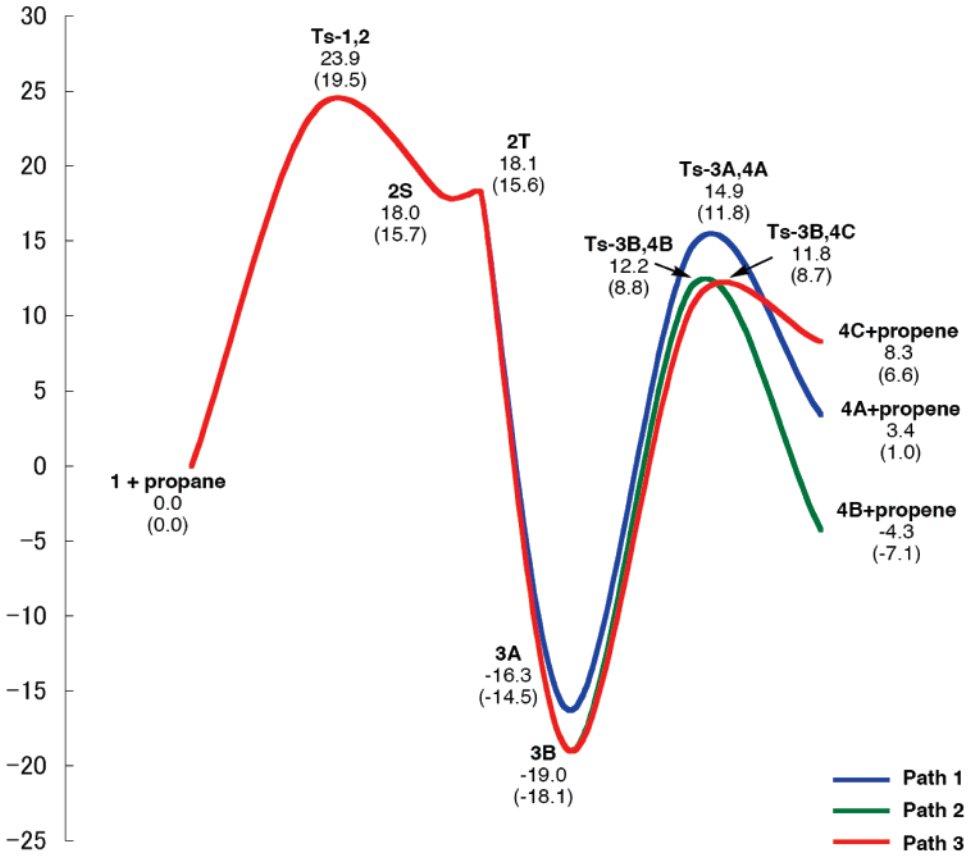


**Figure 6.** Energy profiles for propane ODH on $V_4O_{10}$ (the first row of the energetic parameters is $\Delta E$, while the second row is $\Delta H_{0K} = \Delta E +$ ZPE).

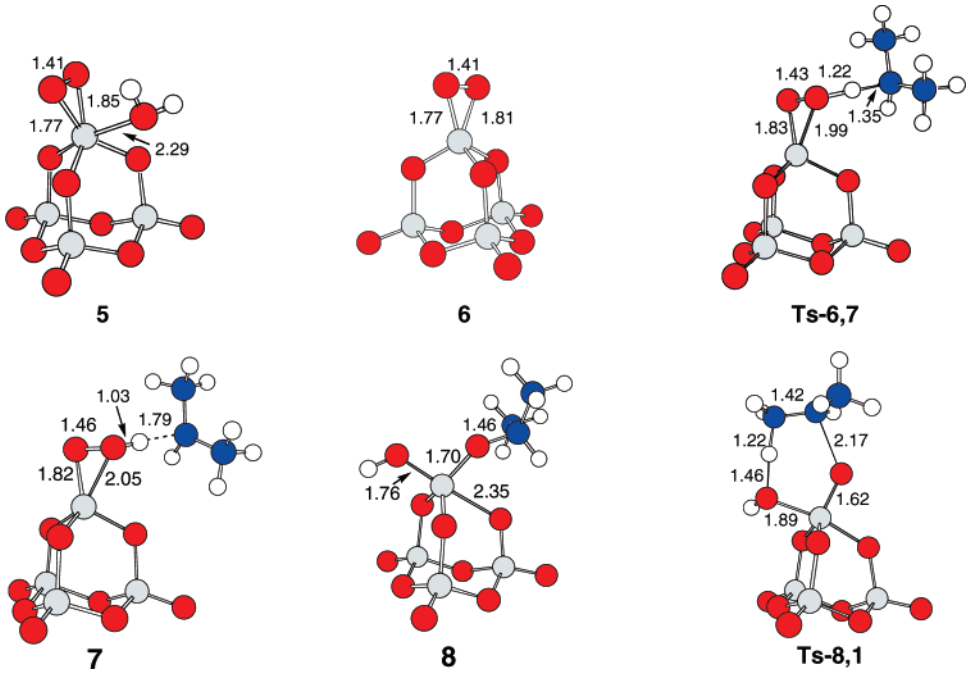


**Figure 7.** Structural parameters for the intermediates and transition states of the vanadium reoxidation step.

coordinated with the empty $d_{yz}$ orbital of the V. This leaves the $d_{z^2}$ and $d_{xz}$ orbitals singly occupied and triplet paired.

*3.4.1. Dissociation of the $H_2O$ from **4C** Is Not Favorable.* It might be expected that water would easily dissociate from **4C** (an $H_2O-V_4O_9$ complex with a $V^{III}$) to create a vacant $V^{III}$ site. However, we calculate a dissociation energy of 37.8 kcal/mol, which is significantly higher than the activation barriers for the conversion of propane to propene. Instead, we explored associative mechanisms where water dissociation is assisted by the oxidant, $O_2$.

*3.4.2. Bonding of $O_2$ to **4C**.* The bond energy of $^3O_2$ to **4C** to form **5**, a complex of $V_4O_{11}$ and water, is 12.2 kcal/mol. Because

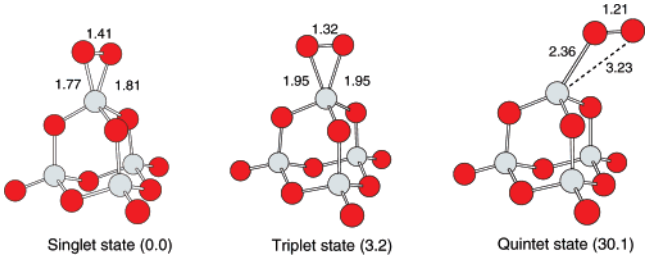


**Figure 8.** The structure parameters and relative energy for the lowest singlet, triplet, and quintet states of **6**. The bond energies relative to free $^3O_2$ and triplet $V_4O_9$ are 37.1, 33.9, and 7.0, respectively.

both $O_2$ and **4C** are triplet states, we can form two singlets, three triplets, and one quintet state. We find that the ground state is the singlet, with the triplet state just 0.1 kcal/mol higher and the quintet state 7.7 kcal/mol higher.

Forming new bonds between such triplet states leads to the loss of one-half the exchange stabilization of the isolated triples, which might be expected to lead to a small barrier. However, the spin couplings can change continuously from that of the separated entities (the GF coupling[48,49]) to that of the molecule (the G1 coupling[48,49]), so that there is no net barrier (as shown by Voter and Goddard[50] for $^3CH_2 + {}^3CH_2$ to form ethene).

Indeed, we could find no barrier for the bonding of dioxygen to **4C**. All attempts at scanning the distance between **4C** and $O_2$ showed a monotonous decrease in energy, eventually resulting in the stable complex **5**, which can be considered as a complex of $V_4O_{11}$ (**6**) and water.

As will be described more completely in our discussion of **6** below, the VOO forms a cyclic peroxide. Taking the VOO plane as *xz*, this involves rehybridizing the $d_{z^2}$ and $d_{xz}$ orbitals on the V to obtain orbitals that can spin pair directly with the $Op_z$ orbitals on each O to form VO bonds, reducing the OO bond order to one. Here, the $H_2O$ lone pair continues to coordinate with the empty $d_{yz}$ orbital of the V, although the V−$OH_2$ bond distance in **5** is 2.29 Å, which is 0.24 Å longer than in **4C**, indicating a dramatically weakened bond.

*3.4.3. Desorption of $H_2O$ from **5** To Form **6**.* Binding $O_2$ to **4C** has the effect of destabilizing the bonding of $H_2O$. Thus, the energy to desorb $H_2O$ from **5** is only 12.9 kcal/mol (rather than the 37.8 kcal/mol from **4C**). Dissociating water from **5** produces the $V_4O_{11}$ cluster **6**, which can be thought of as the result of binding triplet dioxygen ($^3O_2$) to the triplet state of the $V_4O_9$ cluster formed from $V_4O_{10}$ by removing a single O(1) atom. This combination of two triplet states leads to two singlets, three triplets, and one quintet state. Considering the axis of the V═O(1) bond of the original $V_4O_{10}$ cluster as the *z*-axis, this V═O(1) bond can be thought of as a $\sigma$ bond of $Vd_{z^2}$ to $Op_z$ and a $\sigma$ bond of $Vd_{xz}$ to the singly occupied $Op_x$ (double bond in the *xz* plane) with the remaining doubly occupied $Op_y$ orbital overlapping the empty $Vd_{yz}$. There is then resonance between this state with the bond in the *xz* plane and the equivalent state with the bond in the *yz* plane. Thus, the triplet $V_4O_9$ cluster can be considered as having singly occupied $Vd_{z^2}$ and $Vd_{xz}$ (or singly occupied $Vd_{z^2}$ and $Vd_{yz}$) available for binding.

We find that the ground state of **6** has the $O_2$ bonded sideways ($VO_2$ ring) to form a cyclic peroxide with V−O bond distances of 1.77 and 1.81 Å and an O−O bond distance of 1.41 Å, as shown in Figure 8. This suggests a single covalent O−O bond and a single covalent bond between V and each O. Considering the $VO_2$ plane as *xz*, one can think of the bond as formed from hybrids of $Vd_{z^2}$ and $Vd_{xz}$ bonded to the $p_z$ singly occupied orbitals from each of the two O atoms. This leads to a net bond energy for $O_2$ to the $V_4O_9$ cluster in **6** of 37.1 kcal/mol (dissociating to $^3O_2$ and the triplet state of $V_4O_9$).

The triplet state of **6** is only 3.2 kcal/mol higher in energy than the singlet. The 1.32 Å bond length of the triplet indicates a bond order of $^3/_2$, the same as in the $HO_2$ radical (bond distance = 1.33 Å). Indeed, we find that one of the two unpaired electrons is in an OO $\pi^*$ antibonding orbital (*xz* and *yz* nodal planes, leading to *xy* overall symmetry) distributed evenly between the oxygen atoms in the peroxo group, thus forming a 3-electron/2-center O−O bond. The other unpaired spin of the triplet state is in the $VO_2$ plane, but in a $Vd_{xy}$-like orbital. The bonding interaction between the O−O fragment and V can be thought of as a spin pairing of the $O_2$ $\pi^*$ orbital in the *xz* plane with the $Vd_{xz}$ orbital. This leads to three electrons in the *xz* plane between the V and $O_2$, suggesting a net bond order of 1.5. Indeed, the VO bonds of the triplet state are 0.18 and 0.14 Å longer than those of the singlet state, about what one would expect of bonds having $^3/_4$ bond order. The bond is to the $O_2$ $\pi^*$ orbital. Because the fragments of **6** ($O_2$ and $V_4O_9$) both have triplet ground states, we also investigated the quintet state of **6**. However, as this state cannot form bonds between any of the 4 singly occupied orbitals, the quintet state of **6** is 30.1 kcal/mol higher in energy than the singlet state, with a calculated V−$O_2$ bond energy of 7.0 kcal/mol. This state leads to an OO bond distance of 1.21 Å (same as we calculate for a free $^3O_2$) and V−O bond distances of 2.36 and 3.23 Å. Here, the two unpaired spins on the V are $d_{xz}$ and $d_{z^2}$. Thus, one can think of the quintet state as a weakly bound van der Waals complex, with perhaps an electrostatic component due to the quadrupole moment on the $O_2$.

Recently, a V-peroxo moiety was observed experimentally at low temperature (90 K) in the reaction of gaseous $O_2$ with $V_2O_3$(0001) surface, a product of deep reduction of $V_2O_5$.[51] The vibrational frequency observed in the IRAS spectra was 951 $cm^{-1}$ (indicative of a peroxo species). As the temperature was increased, this species disappeared below 225 K and was replaced by a normal V═O(1) frequency at 1040 $cm^{-1}$. We calculate 1042 $cm^{-1}$ for the O−O stretching mode in singlet **6** and 1122−1142 for the three V═O(1) modes. [Our calculated vibrational frequency for the O−O stretching mode in the triplet state is 1233 $cm^{-1}$ and for the quintet state is 1644 $cm^{-1}$ (we calculate 1662 $cm^{-1}$ for the free $O_2$).] Our $V_4O_{10}$ cluster puts the peroxo vibration at 90 $cm^{-1}$ below the V═O(1) stretch, which is in good agreement with the experimental observation on reduced $V_2O_3$ (89 $cm^{-1}$ shift). Consequently, we agree with the assignment by ref 51 of the 951 $cm^{-1}$ species as a peroxo-bound species, V−($O_2^{2-}$). The observation of such an OO species in IRAS has been attributed to the change in the V−O distance as the OO bond is modified.[51]

*3.4.4. Conversion of **6** To Reform the Initial Catalyst, $V_4O_{10}$.* To complete the catalytic cycle, the peroxoy species **6** must be converted back to the initial $V_4O_{10}$ complex. We expected that **6**, with its nearly degenerate singlet and triplet states, would be more reactive than the initial model catalyst, $V_4O_{10}$ (**1**). However, bonding an H atom to **6** to form a bound V−OOH gains 80.3 kcal/mol, as compared to 78.0 kcal/mol for bonding H to the V═O(1) of $V_4O_{10}$ (**1**), indicating similar reactivity. Even so, this is much weaker than the OH bond of $H_2O$

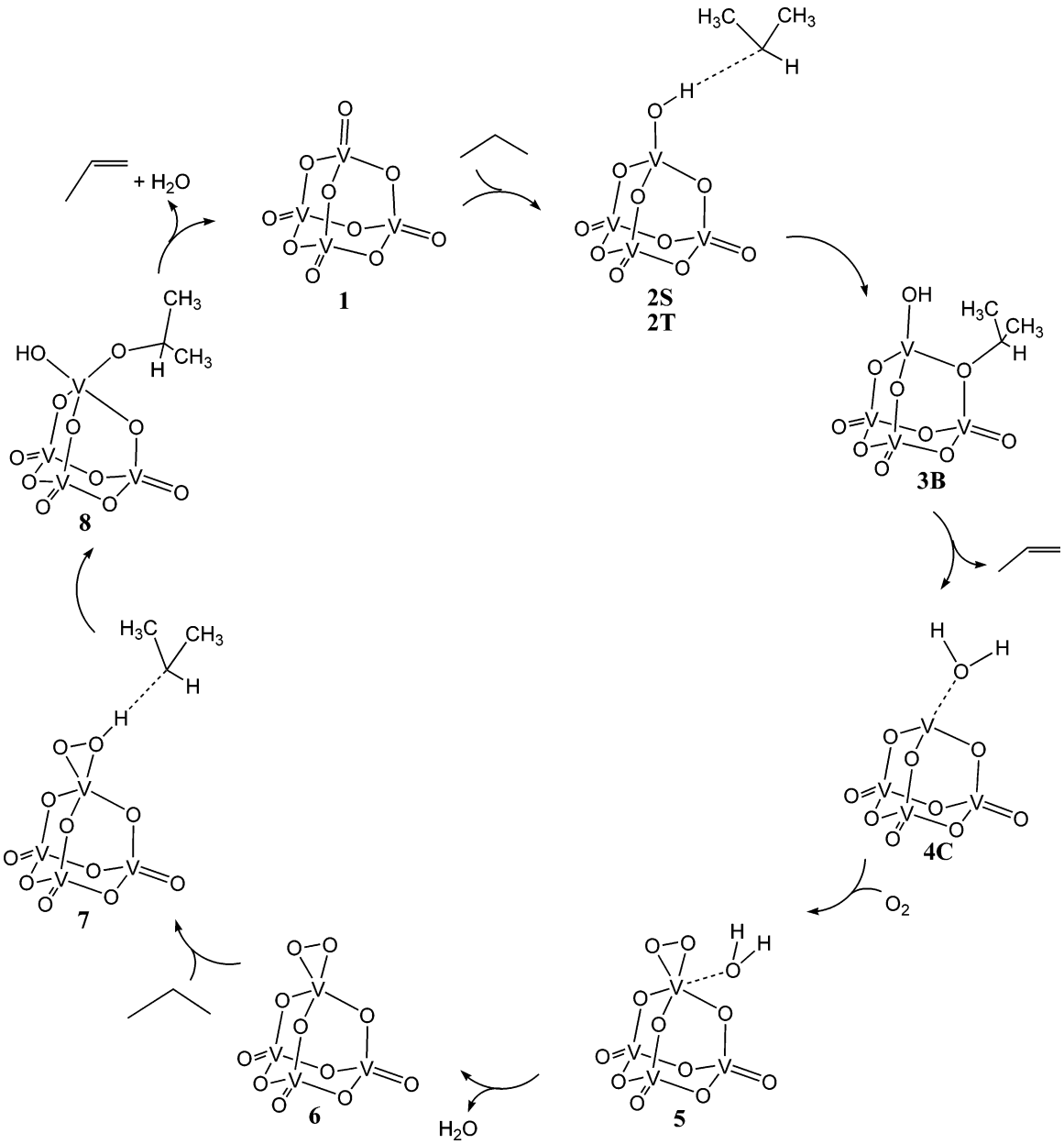


**Figure 9.** The catalytic cycle for propane ODH on $V_4O_{10}$ derived from the QM calculations. The energies are in Figure 10. We refer to this as the single site vanadyl activation, functionalization, and reoxidation mechanism (SS-VAFR).

(calculated to be 119.9 kcal/mol), and consequently we would not expect to find reactions such as sequential hydrogen transfers from water [**6** + $H_2O \rightarrow V_4O_9(OOH)(OH) \rightarrow V_4O_{10}$ + HOOH]. Indeed, experimental studies found no traces of hydrogen peroxide even as a transient intermediate.

Instead, we hypothesized that **6** might instead activate a second propane. We find a very facile mechanism for hydrogen abstraction using the peroxo moiety (peroxo-$H^{1st}$-abs step), with a calculated barrier of 16.5 kcal/mol, 7.4 kcal/mol lower than the barrier for the initial hydrogen abstraction step (**Ts-1,2**) using the $V_4O_{10}$ catalyst. [Because the transition state (**Ts-6,7**) and product (**7**) of this new hydrogen abstraction step have diradical character, the broken symmetry approach was used to calculate the open-shell singlet states.]

In the subsequent step, the iso-propyl radical fragment in **7** bonds with the other oxygen atom of the peroxo group to form **8** without a barrier. The second molecule of propene and water are formed by passing through a six-membered ring transition state, **Ts-8,1**. For this step, the activation energy is 30.0 kcal/mol, and the reaction energy is 29.1 kcal/mol (peroxo-$H^{2nd}$-abs step). At 298.15 K, the Gibbs free energy barrier reduces to 24.2 kcal/mol. The initial $V_4O_{10}$ catalyst is regenerated, completing the catalytic cycle.

**3.5. Catalytic Cycle for Single-Site Vanadyl Activation, Functionalization, and Reoxidation Mechanism (SS-VAFR).** Combining the lowest energy steps from the previous sections, we can now determine the complete catalytic cycle, summarized schematically in Figure 9. The potential energy surface for this cycle is shown in Figure 10. The overall reaction is

$$V_4O_{10} + 2C_3H_8 + O_2 \rightarrow V_4O_{10} + 2C_3H_6 + 2H_2O, \quad \Delta E = -26.0 \text{ kcal/mol}$$

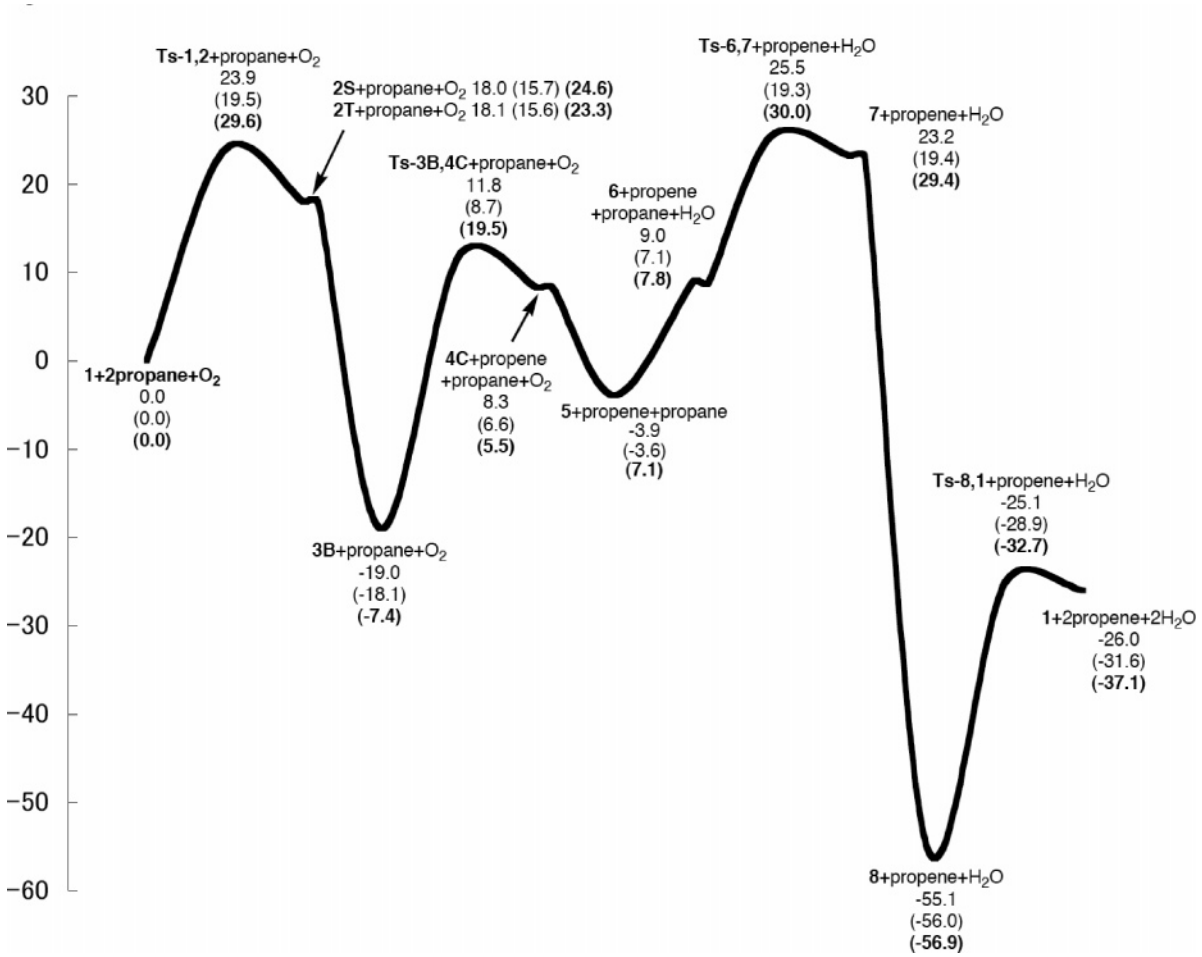


**Figure 10.** Energy profiles of the SS-VAFR catalytic cycle for propane ODH on $V_4O_{10}$ (the first row of the energetic parameters is $\Delta E$, the second row is $\Delta H_{0K} = \Delta E + \text{ZPE}$, and the third low is $\Delta G(298.15\ \text{K})$).

The four reaction barriers (kcal/mol) in this catalytic cycle are

**vanadyl-H$^{1st}$-abs step:**

$$\Delta E = 23.9\ \text{kcal/mol}, \quad \Delta G_{298.15} = 29.6\ \text{kcal/mol}$$

**hydroxyl-H$^{2nd}$-abs step:**

$$\Delta E = 30.8\ \text{kcal/mol}, \quad \Delta G_{298.15} = 26.9\ \text{kcal/mol}$$

**peroxo-H$^{1st}$-abs step:**

$$\Delta E = 16.5\ \text{kcal/mol}, \quad \Delta G_{298.15} = 22.2\ \text{kcal/mol}$$

**peroxo-H$^{2nd}$-abs step:**

$$\Delta E = 30.0\ \text{kcal/mol}, \quad \Delta G_{298.15} = 24.2\ \text{kcal/mol}$$

Thus, although the highest barrier on the $\Delta E$ surface is 30.8 kcal/mol for hydroxyl-H$^{2nd}$-abs step, the free energy barrier at 298.15 K (rate-determining) is activating the methylene C−H bond of propane (vanadyl-H$^{1st}$-abs step). This is consistent with experiments.[12,13,19]

In our catalytic cycle, the V═O(1) is the active site for all steps with O(2) only playing the role of stabilizing the isopropyl radical by forming the stable intermediate **3B**. Thus, we refer to this as the single-site vanadyl activation, functionalization, and reoxidation (SS-VAFR) mechanism. The SS-VAFR mechanism is appropriate for describing the propane ODH reaction on supported vanadium oxide catalysts where it is expected that only isolated monovanadates species are present with are no adjacent V−O(2)−V or V═O(1) groups. Particularly interesting is that this novel mechanism accounts for reoxidation of the reduced vanadium center with simultaneous dissociation of water to generate a V-peroxo moiety with higher reactivity than the original V═O(1).

## 4. Comparisons with Previous Computational Studies

Previous theoretical investigations of $V_2O_5(001)$ surface by Hermann et al.[52] suggested that the water dissociation energy could be decreased by forming bonds between the reduced V atom and the V═O(1) group of the second layer. However, the supported vanadium oxide catalysts have vanadia concentrations of less than the one monolayer limit, with structures that do not have the layered structure suggested to facilitate water dissociation. Our current calculations do not allow us to directly compare the two possible pathways, but instead we provide an alternative way to reoxidize the reduced vanadium center and remove water from the surface simultaneously without the need to postulate assistance of bonding between layers in $V_2O_5(001)$.

**4.1. Energetics of H−O Bond Formation.** Hermann et al.[52] studied binding energies of hydrogen on $V_2O_5$ using the Zhang−Yang modification (rev-PBE)[53] of the PBE DFT to calculate single point energies on structures optimized with the Vosko−Wilk−Nusair LDF functional. They calculated the binding energy of hydrogen atoms to the three different types of oxygen atoms on a one-layer $V_2O_5(001)$ cluster model containing 5 formula units terminated by hydroxyl groups, and concluded

that the bond strength is 54.0 kcal/mol with O(1), 51.0 kcal/mol with O(2), and 43.4 kcal/mol with O(3).

Yin et al.[54] performed periodic BLYP calculations on a one-layer periodic $V_2O_5$(001) slab. They also found a similar trend in bond strengths of the hydrogen atom to the different oxygen types: 62.2 kcal/mol with O(1), 60.3 kcal/mol with O(2), and 59.3 kcal/mol with O(3). However, the difference between the O(1)−H and O(3)−H bond strengths is calculated to 2.9 kcal/mol, rather than 10.6 kcal/mol, as calculated by Hermann et al.[52]

Fu et al.[22] also performed periodic QM calculations, using the GGA-PW91 flavor of DFT, on a one-layer periodic $V_2O_5$-(001) slab to determine the strength of the H−O bond. They found a trend consistent with Yin[54] and Hermann[52] and calculated the energy of adsorption of the H atom on O(1) = 66.3 kcal/mol, on O(2) = 61.2 kcal/mol, and on O(3) = 58.0 kcal/mol. [Their reported numbers were O(1) = 12.7 kcal/mol, on O(2) = 7.6 kcal/mol, and on O(3) = 4.4 kcal/mol relative to $^1/_2H_2$. We converted this to values relative to H atom using the PW91 bond energy for $H_2$ of 107.1 kcal/mol.] Thus, here the difference between the O(1)−H and O(3)−H bond strengths is 8.3 kcal/mol, in between the values from Yin[54] and Hermann.[52]

Our HO bond energies are 78.0 for O(1) and 69.5 kcal/mol for O(2), which are both ∼20 kcal/mol higher than the energies reported by Herman et al.,[52] and ∼10 kcal/mol higher than those by Fu et al.[22] As a first test for the origin of this difference, we explored the effect of increasing the size of the basis set.

When using the 6-311G** basis functions for the H, C, and O atoms (along with the LACV3P effective core potential and double-$\zeta$ basis on the V), but leaving out the polarization functions on the H's, we find a 1.3 kcal/mol increase in the two binding energies to 79.3 and 70.8 kcal/mol, respectively, implying that increasing the quality of the basis sets does not significantly change the binding energies.

We next tested the DFT functionals, by recalculating the HO bond energies with the PBE and PW91 functionals and comparing to those of Herman et al.[52] and Fu et al.[22]

The PBE functional yielded HO bond energies of 68.6 kcal/mol for O(1) and 61.4 kcal/mol for O(2) (10.7 and 9.4 kcal/mol smaller than B3LYP), which can be compared to Hermann's values of 54.0 kcal/mol for O(1) and 51.0 kcal/mol for O(2) using rev-PBE.[52] While the difference between the two functionals was reduced by ∼50%, the remaining difference is still unaccounted for and may be a peculiarity of rev-PBE or of their cluster model.

With the PW91 functional, we find HO bond energies of 71.3 kcal/mol for O(1) and 63.9 kcal/mol for O(2) (8.0 and 6.9 kcal/mol weaker than for B3LYP). This can be compared to Fu's values of H−O(1) = 66.3 kcal/mol and H−O(2) = 61.2 kcal/mol.[22] This remaining difference may be a difference between their single periodic layer model and our cluster model.

It is not yet clear whether our results or those of Herman et al.[52] or Fu et al.[22] are most accurate. However, our calculations are all based on the B3LYP flavor of DFT, which gives the average errors in cohesive energies of 3.1 kcal/mol for the G2 set, as compared to average errors of 17.1 and 17.8 for PBE and PW91.[55,56]

More to the point for this project, the H−OH bond energy is calculated to 119.9, 121.8, and 122.2 kcal/mol for B3LYP, PBE, and PW91, respectively, which can be compared to the experimental value of $D_e$ = 125.8 kcal/mol.[57]

Similarly, the $CH_3$−OH bond energy is calculated to be 96.0, 103.2, and 103.5 kcal/mol for B3LYP, PBE, and PW91, respectively, which can be compared to the experimental value of $D_e$ = 98.3 kcal/mol.[57]

The $C_2H_5$−OH bond energy is 96.0, 102.7, and 103.1 kcal/mol for B3LYP, PBE, and PW91, respectively, which can be compared to the experimental value of $D_e$ = 99.3 kcal/mol.[57]

Averaging the results for H−OH, $CH_3$−OH, and $C_2H_5$−OH, we expect the errors with B3LYP, PBE, and PW91 for H−OH or C−OH bonds to be 3.8, 4.1, and 4.2 higher than the corresponding experimental values, respectively. Thus, we expect our B3LYP energies should be the most accurate. Nevertheless, this accounts for only about one-half the discrepancy with these previous calculations.

Finally, all calculations agree that it is easier to bond the H to V═O(1) than to V−O(2)−V, as expected from having a weaker V═O $\pi$ bond. The differences are 8.5 kcal/mol in our work, 3.0 for Hermann,[52] and 1.9 for Yin.[54]

**4.2. Energetics of O Removal.** Sauer et al.[42,58] calculated the energy for formation of an oxygen vacancy using both a two-layer cluster (10 formula units terminated with hydroxyl groups) and a two-layer periodic slab (12 formula units per cell). They used the PW91 flavor of DFT for periodic calculations[42] and BP86, B3LYP, and PBE flavors of DFT for cluster calculations.[58] The V═O bond dissociation energy in $VO_2^+$ calculated using hybrid DFT (B3LYP) provided the best results and was within 4 kcal/mol of experiment, while gradient corrected but nonhybrid functionals (BP86 and PBE) yielded large errors of 18.0−37.0 kcal/mol. They concluded from the periodic slab calculations that the energy to remove O(1) is 45.0 kcal/mol, O(2) is 84.9 kcal/mol, and O(3) is 90.9 kcal/mol.[42] In contrast, they found that the finite cluster leads to an oxygen vacancy energy of 27.0 kcal/mol for removal of O(1).[58] They attributed the ease of removing oxygens from the two-layer slab to the formation of V−O−V bonds between the crystal layers.

Hermann et al.[52] calculated the energy to form an oxygen vacancy using a one-layer model consisting of 5 $V_2O_5$ formula units terminated by hydrogen atoms. Using rev-PBE, they found that the energy to remove O(1) is 149.2 kcal/mol, O(2) is 165.8 kcal/mol, and O(3) is 149.7 kcal/mol.

We also calculated the energy for formation of an oxygen vacancy in the $V_4O_{10}$ cluster and found that energy to remove O(1) is 121.9 kcal/mol and O(2) is 140.2 kcal/mol using the B3LYP level. The difference between this and the results of Sauer (also B3LYP)[58] is most likely due to the second layer that they include.

To compare with Hermann, we also carried out PBE calculations obtaining values of 145.8 kcal/mol for O(1) and 173.2 kcal/mol for O(2), in rough agreement with Hermann.[52] This suggests that the difference between our results and the Hermann results is due to our using a more accurate level of DFT. Nevertheless, while the two-layer periodic slab has significantly smaller values, the qualitative trend in the oxygen vacancy energy is consistent for the different $V_2O_5$ systems.

**4.3. Removal of an OH Bond.** Hermann et al.[52] found that the energy to remove a hydroxyl group, formed by adding a hydrogen atom to the O(1), O(2), and O(3) of a one-layer model (consisting of 5 formula units terminated with hydrogen atoms), was 91.8, 105.4, and 81.6 kcal/mol, respectively.

The one-layer periodic calculations of Yin et al.[54] also reveal the same trend in binding energies of the hydroxyl group, with 94.5 kcal/mol for removal of O(1)H, 109.0 kcal/mol for removal of O(2)H, and 88.0 for removal of O(3)H.

We find that the strength of the V−OH bond using the $V_4O_{10}$ model is 94.3 kcal/mol for O(1)H and 104.1 kcal/mol for O(2)H, which is consistent with both Hermann's[52] and Yin's[54] results.

**4.4. Removal of a Surface $H_2O$.** Hermann et al.[52] calculated the energy to remove water formed at an O(1) to be 11.1 kcal/mol, at an O(2) to be 3.7 kcal/mol, and at an O(3) to be −10.1 kcal/mol. Therefore, the energy for oxygen removal is reduced by as much as 40% via dissociation of a hydroxyl group and 90% through dissociation of water when compared to removal of an oxygen atom.

We also calculated the strength of the $V-OH_2$ bond using the $V_4O_{10}$ cluster and found the strength of the $V-O(1)H_2$ bond to be 37.8 kcal/mol and the strength of the $V-O(2)H_2$ to be 5.4 kcal/mol. Our binding energy for $V-O(1)H_2$ is very different from that of Hermann,[52] who obtains 11.1 kcal/mol. However, it is not clear what is the origin of this discrepancy. Single point PBE calculations using geometries optimized for B3LYP give a $V-O(1)H_2$ bond energy of 34.5 kcal/mol, and similarly calculations on $Cl_3V-OH_2$ give 36.0 kcal/mol for B3LYP and 34.0 kcal/mol for PBE. This indicates that the discrepancy is not due to the functional. Moreover, all our calculated clusters fully relax the symmetry, and we have ensured that all lowest energy orbital populations have been used.

We find that the triplet state for the species $V_4O_9-O(1)H_2$ is 22.3 below the singlet, while for $V_4O_9$ the triplet is 15.0 kcal/mol below the single. It is possible that Hermann et al.[52] used the singlet state for the water complex (nothing is mentioned about spin in the paper). If so, they would obtain an overall binding energy far too small. Thus, for B3LYP, we calculate that $V_4O_9-H_2O$ (singlet state) → $V_4O_9$ (triplet state) + $H_2O$ is uphill by 15.5 kcal/mol.

Moreover, the Fu's two-layers periodic calculations[22] that lead to $V-H_2O$ binding energy is 13.0 kcal/mol with the assistance of an extra V−O−V bond between the two layers. It is reasonable to assume that the $V-H_2O$ binding energy will increase, if only one-layer periodic model is used. Although there is discrepancy between our results and Hermann's,[52] both calculations agree that the presence of hydrogen on the $V_2O_5$-(001) surface facilitates removal of $H_2O$ from the surface.

**4.5. Reaction Mechanism.** Several recent theoretical papers have provided new insight into the alkane ODH mechanism.[20−22] Gilardoni et al.[20] used DFT (BPW91 flavor) to investigate the propane ODH reaction mechanism on finite clusters. It is found that the initial step is a barrierless O(1) insertion into the C−H bond of the propane methylene group and that the highest barrier for conversion of propane to propene (15 kcal/mol) arises from hydrogen migration from the methyl group in absorbed iso-propyl to protonated O(3) to form water. Redfern et al.[21] re-examined this mechanism using a different $V_2O_5$ model and found a 79.4 kcal/mol barrier for the O(1) insertion into the C−H bond and an overall barrier of 80.5 kcal/mol for the reaction pathway. For this reason, Redfern et al.[21] concluded that the $V_2O_5$(001) surface is unfavorable for propane ODH, contradicting Gilardoni's[20] results.

However, several potential mechanistic pathways were left unexplored in the previous studies, particularly the direct hydrogen abstraction leading to a propyl radical. Our studies on a finite cluster model find that this mechanism is quite feasible. We find that the energetically most favorable activation of propane occurs through hydrogen abstraction of the methylene hydrogen by a vanadyl group with a barrier of 23.9 kcal/mol. We find that the highest $\Delta E$ barrier for the overall mechanism is 30.8 kcal/mol, corresponding to extraction of the second H from the $CH_3$ of iso-propyl bonded to O(2) by the OH bonded to the original O(1) site that activated the propane.

While this manuscript was in preparation, a paper by Fu et al.[22] appeared that also considered ODH, but using periodic DFT calculations (PBE rather than B3LYP) on a periodic slab with one layer of $V_2O_5$(001).

They found that the vanadyl-$H^{1st}$-abs step is most favorable with a $\Delta E$ barrier of 27.3 kcal/mol, in agreement with our conclusion and with a quantitative result quite similar to our value of 23.9 kcal/mol. Thus, both our results and those of Fu et al.[22] contradict the conclusions from Gilardoni et al.[20] and Redfern et al.[27] that activation occurs by O(1) insertion into the C−H bond of propane.

Fu et al. also proposed an alternative C−H activation pathway of O(2) insertion into the methylene C−H bond propane, reporting a $\Delta E$ barrier of 30.4 kcal/mol. We did not consider this pathway for propane ODH on the $V_4O_{10}$ model, as we assumed that such a direct insertion would have a prohibitively high barrier.

Fu et al.[22] described two mechanisms for abstraction of the second hydrogen from one of the methyl groups of the chemisorbed iso-propyl. Mechanism Fu-1 uses a second O(1) to abstract hydrogen from an iso-propyl group bonded to a second O(1) with a calculated $\Delta E$ barrier of 30.9 kcal/mol. Mechanism Fu-2 uses an O(3) to abstract a hydrogen from an iso-propyl group bonded to O(2) with a barrier of $\Delta E = 33.7$ kcal/mol. Fu did not consider the process that we find most favorable (30.8 kcal/mol barrier), extraction of the second H from the $CH_3$ of iso-propyl bonding to O(2) by the OH bonded to the original O(1) site that activated the propane. We did not consider the Fu mechanisms because it does not seem plausible for the $V_4O_{10}$ cluster geometry. For mechanism Fu-1, the distance between two O(1) atoms in the $V_4O_{10}$ model is 5.62 Å, much longer than that of 3.56 Å in $V_2O_5$(001) surface. Moreover, the two V═O(1) groups are not parallel in the $V_4O_{10}$ model, and we do not believe that a mechanism using this geometry would be realistic. Mechanism Fu-2 involves O(3), which does not exist in our $V_4O_{10}$ cluster model.

Nevertheless, the most favorable $\Delta E$ barrier for abstracting the second barrier using a second O(1) that Fu et al. calculate (30.9 kcal/mol) is quite similar to our most favorable $\Delta E$ barrier (30.8 kcal/mol) using the O(1)H.

We consider that our mechanism is probably relevant for supported $V_2O_5$ catalysts where the O(1) sites are likely isolated. For bulk $V_2O_5$ catalysts, Sauer[42,58] has shown that there are major effects due to the second layer of $V_2O_5$, and hence the Fu mechanisms (based on a single layer) might not be relevant here.

## 5. Conclusions

We conclude from the consistency of these studies with experimental mechanistic results that the cubic $V_4O_{10}$ cluster is a valid model for studying the catalysis on $V_2O_5$, particularly for supported catalysts, which have only separated monovanadate ($VO_4$) species. The advantage over other cluster models is that there are no broken bonds to O and no OH groups, each of which can affect the energies and mechanism. However, we have not shown that this model describes the chemistry of the bulk catalyst where effects involving the second layer could play a role.

We report here the complete catalytic cycle for conversion of propane to propene on a $V_4O_{10}$ cluster including reoxidation of the active site. This is the single-site vanadyl activation, functionalization, and reoxidation mechanism (SS-VAFR).

At 298.15 K, we find that the rate-determining step (highest barrier of 29.6 kcal/mol) corresponds to the first hydrogen abstraction from the methylene group of propane by the terminal oxygen (V═O(1)). This is consistent with experimental re-

sults.[12,13,19] Particularly remarkable about our catalytic cycle is that gaseous $^3O_2$ promotes water desorption while simultaneously reoxidizing the reduced vanadium oxide catalyst. Without this promotion by $^3O_2$, the barrier for water dissociation would increase significantly from 12.9 to 37.8 kcal/mol! Indeed, the resulting peroxo-$V_4O_9$ cluster (**6**) has been observed experimentally.[51] We predict that **6** activates the methylene C−H bond in propane with a reaction barrier 7.4 kcal/mol lower than for the $V_4O_{10}$ cluster. Experiments on this now isolated system would provide an interesting test of our predictions.

Because the C−H bond of propene product is ∼7 kcal/mol weaker than the H−iPr bond in propane, the V═O(1) sites could react more quickly with product than reactant, likely leading to products such as $CO_2$. To avoid such a loss in selectivity, it may be important that the product not be exposed to V═O sites. This may be why the supported catalysts have high selectivity. In the SS-VAFR catalytic cycle, the V═O(1) sites play the essential role for all reaction steps, while bridging oxygens (V−O(2)−V) play the role stabilizing the iso-propyl intermediate. This mechanism should be most suitable for understanding the propane ODH reaction on supported vanadium oxide catalysts, where only monovanadates species are expected to be present.

**Acknowledgment.** The personnel involved in this research were partially supported by DOE (DE-PS36-03GO93015), ONR (N00014-06-1-0938), and Chevron. The facilities were supported by ARO-DURIP and ONR-DURIP funds.

**Supporting Information Available:** Computational details, including the Cartesian coordinates and total energies for the structures calculated and vibrational frequencies for selected cases. This material is available free of charge via the Internet at http://pubs.acs.org.

## References and Notes

(1) Le Bars, J.; Vedrine, J. C.; Auroux, A.; Trautmann, S.; Baerns, M. *Appl. Catal., A* **1992**, *88*, 179.

(2) Blasco, T.; Nieto, J. M. L. *Appl. Catal., A* **1997**, *157*, 117.

(3) Surnev, S.; Ramsey, M. G.; Netzer, F. P. *Prog. Surf. Sci.* **2003**, *73*, 117.

(4) Went, G. T.; Oyama, S. T.; Bell, A. T. *J. Phys. Chem.* **1990**, *94*, 4240.

(5) Oyama, S. T.; Somorjai, G. A. *J. Phys. Chem.* **1990**, *94*, 5022.

(6) Oyama, S. T.; Middlebrook, A. M.; Somorjai, G. A. *J. Phys. Chem.* **1990**, *94*, 5029.

(7) Oyama, S. T. *J. Catal.* **1991**, *128*, 210.

(8) Le Bars, J.; Vedrine, J. C.; Auroux, A.; Pommier, B.; Pajonk, G. M. *J. Phys. Chem.* **1992**, *96*, 2217.

(9) Kung, H. H. *Adv. Catal.* **1994**, *40*, 1.

(10) Busca, G. *Catal. Today* **1996**, *27*, 457.

(11) Khodakov, A.; Olthof, B.; Bell, A. T.; Iglesia, E. *J. Catal.* **1999**, *181*, 205.

(12) Chen, K. D.; Khodakov, A.; Yang, J.; Bell, A. T.; Iglesia, E. *J. Catal.* **1999**, *186*, 325.

(13) Chen, K. D.; Iglesia, E.; Bell, A. T. *J. Catal.* **2000**, *192*, 197.

(14) Argyle, M. D.; Chen, K. D.; Bell, A. T.; Iglesia, E. *J. Catal.* **2002**, *208*, 139.

(15) Argyle, M. D.; Chen, K. D.; Bell, A. T.; Iglesia, E. *J. Phys. Chem. B* **2002**, *106*, 5421.

(16) Pieck, C. L.; Banares, M. A.; Fierro, J. L. G. *J. Catal.* **2004**, *224*, 1.

(17) Mamedov, E. A.; Corberan, V. C. *Appl. Catal., A* **1995**, *127*, 1.

(18) Mars, P.; van Krevelen, D. W. *Chem. Eng. Sci., Special Suppl.* **1954**, *3*, 41.

(19) Chen, K. D.; Bell, A. T.; Iglesia, E. *J. Phys. Chem. B* **2000**, *104*, 1292.

(20) Gilardoni, F.; Bell, A. T.; Chakraborty, A.; Boulet, P. *J. Phys. Chem. B* **2000**, *104*, 12250.

(21) Redfern, P. C.; Zapol, P.; Sternberg, M.; Adiga, S. P.; Zygmunt, S. A.; Curtiss, L. A. *J. Phys. Chem. B* **2006**, *110*, 8363.

(22) Fu, H.; Liu, Z.-P.; Li, Z.-H.; Wang, W.-N.; Fan, K.-N. *J. Am. Chem. Soc.* **2006**, *128*, 11114.

(23) Becke, A. D. *J. Chem. Phys.* **1993**, *98*, 5648.

(24) Becke, A. D. *Phys. Rev. A* **1988**, *38*, 3098.

(25) Lee, C. T.; Yang, W. T.; Parr, R. G. *Phys. Rev. B* **1988**, *37*, 785.

(26) Baker, J.; Muir, M.; Andzelm, J.; Scheiner, A. In *Chemical Applications of Density Function Theory*; Laird, B. B., Ross, R. B., Ziegler, T., Eds.; ACS Symposium Series 629; American Chemical Society: Washington, DC, 1996.

(27) Niu, S. Q.; Hall, M. B. *Chem. Rev.* **2000**, *100*, 353.

(28) Oxgaard, J.; Periana, R. A.; Goddard, W. A., III. *J. Am. Chem. Soc.* **2004**, *126*, 11658.

(29) Benitez, D.; Goddard, W. A., III. *J. Am. Chem. Soc.* **2005**, *127*, 12218.

(30) Keith, J. M.; Nielsen, R. J.; Oxgaard, J.; Goddard, W. A., III. *J. Am. Chem. Soc.* **2005**, *127*, 13172.

(31) Jacob, T.; Goddard, W. A., III. *J. Phys. Chem. B* **2005**, *109*, 297.

(32) Keith, J. A.; Oxgaard, J.; Goddard, W. A., III. *J. Am. Chem. Soc.* **2006**, *128*, 3132.

(33) Ziatdinov, V. R.; Oxgaard, J.; Mironov, O. A.; Young, K. J. H.; Goddard, W. A., III; Periana, R. A. *J. Am. Chem. Soc.* **2006**, *128*, 7404.

(34) Nielsen, R. J.; Goddard, W. A., III. *J. Am. Chem. Soc.* **2006**, *128*, 9651.

(35) Oxgaard, J.; Bhalla, G.; Periana, R. A.; Goddard, W. A., III. *Organometallics* **2006**, *25*, 1618.

(36) Persson, P.; Lundqvist, M. J.; Ernstorfer, R.; Goddard, W. A., III; Willig, F. *J. Chem. Theory Comput.* **2006**, *2*, 441.

(37) (a) Hay, P. J.; Wadt, W. R. *J. Chem. Phys.* **1985**, *82*, 299. (b) Melius, C. F.; Goddard, W. A., III. *Phys. Rev. A* **1974**, *10*, 1541. (c) Melius, C. F.; Olafson, B. O.; Goddard, W. A., III. *Chem. Phys. Lett.* **1974**, *28*, 457.

(38) Harihara, P. C.; Pople, J. A. *Chem. Phys. Lett.* **1972**, *16*, 217.

(39) Francl, M. M.; Pietro, W. J.; Hehre, W. J.; Binkley, J. S.; Gordon, M. S.; Defrees, D. J.; Pople, J. A. *J. Chem. Phys.* **1982**, *77*, 3654.

(40) Jaguar 6.5; Schrodinger, LLC: Portland, OR, 2005. The LACV3P** basis set in Jaguar uses the Wadt and Hay core-valence effective core potential with the valence double-ζ contraction of the basis function used for vanadium atom, while 6-311G** basis functions are used for H, C, and O atoms.

(41) Enjalbert, R.; Galy, J. *Acta Crystallogr., Sect. C: Cryst. Struct. Commun.* **1986**, *42*, 1467.

(42) Ganduglia-Pirovano, M. V.; Sauer, J. *Phys. Rev. B* **2004**, *70*, 045422.

(43) Gilson, T. R.; Bizri, O. F.; Cheetham, N. *J. Chem. Soc., Dalton Trans.* **1973**, 291.

(44) Oyama, S. T.; Went, G. T.; Lewis, K. B.; Bell, A. T.; Somorjai, G. A. *J. Phys. Chem. A* **1989**, *93*, 6786.

(45) Kenny, N.; Kannewur, C. R.; Whitmore, D. H. *J. Phys. Chem. Solids* **1966**, *27*, 1237.

(46) Bodo, Z.; Hevesi, I. *Phys. Status Solidi* **1967**, *20*, K45.

(47) Feyel, S.; Dobler, J.; Schroder, D.; Sauer, J.; Schwarz, H. *Angew. Chem., Int. Ed.* **2006**, *45*, 4681.

(48) Goddard, W. A., III. *Phys. Rev.* **1967**, *157*, 73.

(49) Goddard, W. A., III. *Phys. Rev.* **1967**, *157*, 81.

(50) Voter, A. F.; Goodgame, M. M.; Goddard, W. A., III. *Chem. Phys.* **1985**, *98*, 7.

(51) Abu Haija, M.; Guimond, S.; Romanyshyn, Y.; Uhl, A.; Kuhlenbeck, H.; Todorova, T. K.; Ganduglia-Pirovano, M. V.; Dobler, J.; Sauer, J.; Freund, H. *J. Surf. Sci.* **2006**, *600*, 1497.

(52) Hermann, K.; Witko, M.; Druzinic, R.; Tokarz, R. *Appl. Phys., A* **2001**, *72*, 429.

(53) Zhang, Y.; Yang, W. *Phys. Rev. Lett.* **1998**, *80*, 890.

(54) Yin, X. L.; Han, H. M.; Endou, A.; Kubo, M.; Teraishi, K.; Chatterjee, A.; Miyamoto, A. *J. Phys. Chem. B* **1999**, *103*, 1263.

(55) Xu, X.; Goddard, W. A., III. *Proc. Natl. Acad. Sci. U.S.A.* **2004**, *101*, 2673.

(56) Xu, X.; Zhang, Q. S.; Muller, R. P.; Goddard, W. A., III. *J. Chem. Phys.* **2005**, *122*, 014105.

(57) Experimetal bond dissociation energies were obtained from the *CRC Handbook of Chemistry and Physics* (87th ed.), and then back-corrected to 0 K using theoretical temperature corrections (B3LYP/6-31G** level of theory).

(58) Sauer, J.; Dobler, J. *Dalton Trans.* **2004**, 3116.